Biosensors and Bioelectronics 85 (2016) 363–370

Contents lists available at ScienceDirect

Biosensors and Bioelectronics

journal homepage: www.elsevier.com/locate/bios

Silicon nanowire based biosensing platform for electrochemical sensing of Mebendazole drug activity on breast cancer cells

Hani Shashaani [a,b,1], Mahsa Faramarzpour [a,b,1], Morteza Hassanpour [a,b,2], Nasser Namdar [a,b,2], Alireza Alikhani [a,b], Mohammad Abdolahad [a,b,*,1]

[a] Nano Electronic Center of Excellence, Nano Bio Electronic Devices Lab, School of Electrical and Computer Eng, University of Tehran, P.O. Box 14395/515, Tehran, Iran

[b] Nano Electronic Center of Excellence, Thin Film and Nanoelectronic Lab, School of Electrical and Computer Eng, University of Tehran, P.O. Box 14395/515, Tehran, Iran

ARTICLE INFO

Article history:
Received 16 February 2016
Received in revised form
23 April 2016
Accepted 25 April 2016
Available online 9 May 2016

Keywords:
Cancer cell
Electrochemical response
Silicon nanowire
Mebendazole drug
Cyclic voltammetry
Biosensor

ABSTRACT

Electrochemical approaches have played crucial roles in bio sensing because of their Potential in achieving sensitive, specific and low-cost detection of biomolecules and other bio evidences. Engineering the electrochemical sensing interface with nanomaterials tends to new generations of label-free biosensors with improved performances in terms of sensitive area and response signals. Here we applied Silicon Nanowire (SiNW) array electrodes (in an integrated architecture of working, counter and reference electrodes) grown by low pressure chemical vapor deposition (LPCVD) system with VLS procedure to electrochemically diagnose the presence of breast cancer cells as well as their response to anticancer drugs. Mebendazole (MBZ), has been used as antitubulin drug. It perturbs the anodic/cathodic response of the cell covered biosensor by releasing Cytochrome C in cytoplasm. Reduction of cytochrome C would change the ionic state of the cells monitored by SiNW biosensor. By applying well direct bioelectrical contacts with cancer cells, SiNWs can detect minor signal transduction and bio recognition events, resulting in precise biosensing. Our device detected the trace of MBZ drugs (with the concentration of 2 nM) on electrochemical activity MCF-7 cells. Also, experimented biological analysis such as confocal and Flowcytometry assays confirmed the electrochemical results.

1. Introduction

Electrochemical biosensors transduce biological interactions into detectable electrochemical signals (Turner et al., 1987). Biological recognitive markers (e.g., enzymes, aptamers or antibodies) could be immobilized/integrated at the electrochemical interface to mediate the sensing procedure (Gupta and Chaudhury, 2007; Hepel and Zhong, 2012). However, complexity of chemical modifications and non-specific binding, reduced the reliability and commerciality of such biosensors. If label free interactions could be applied between analytes and interface, usage of such sensors in wide variety of bio applications would be developed. Such binding must induce changing in electrochemical signal of redox reporter. Moreover if the oxidative/reductive electrochemical responses of the analyte were unique for different biological transformations (such as metastatic progression states of a cancer cell), we would achieve to sensing patterns without any requirements to complex functionalizations.

In recent years, some generations of Label free Electro-chemical biosensors were developed and shed new lights in bio analysis owing to their low cost, multiplexed detection capabilities, as well as ease of miniaturization without any additional biochemical processes (Kimmel et al., 2012; Kong et al., 2014; Guo et al., 2013). Engineering the bioelectrochemical sensing interface is crucial in such devices due to the impact of an accurate and stable response. Among various surface treatments used in interfacial modification, Applying nanomaterials presented many unique performances depend on their sizes and shapes. Great electrical conductivity, enlarged interactive surface area and well physiochemical interactions are some of the characteristics reported for many nanostructures ranged between metallic NPs to carbon nanotubes (Hosseini et al., 2016; Hepel and Zhong, 2012; Jacobs et al., 2010; Li et al., 2014).

Moreover, if the biocompatibility of nanostructures would be acceptable, sensing interfaces produced by nanostructures, would

* Corresponding author.
E-mail address: m.abdolahad@ut.ac.ir (M. Abdolahad).
[1] Authors with same collaboration.
[2] Authors with same collaboration.

http://dx.doi.org/10.1016/j.bios.2016.04.081
0956-5663/

present new generation of label free biosensors for monitoring vital cells.

SiNWs were noticeably considered in biosensing approaches, between various biocompatible nanomaterials, because of their greatly controllable conductivity with good electron transport properties (Qu et al., 2009; Bauer et al., 2007), enlarged electrochemically active area and well compatibility with silicon fabrication processes (Chen et al., 2011). Well attachment of the cells to the outer wall of such nanostructures was also indicated (Qi et al., 2009; Abdolahad et al., 2013; Prinz, 2015) Many electrical biosensors were developed based on SiNW arrays such as SiNW bioFET (Abdolahad et al., 2014a) and SiNW-ECIS for cancer cell detection as well as SiNW kinked transistor for signal extraction from cardiomyocyte cells (Qing et al., 2014).

Here we attempted to apply SiNW based electrochemical biosensor with integrated Reference and counter electrodes in interaction with cancer cells to assay the presence of cancer cells and effect of anticancer drugs on the cell vitality by monitoring the anodic/cathodic current peaks of the cell covered SiNWs. The 75 μm WE covered by VLS grown forest shaped SiNW structures applied to increase the interactive surface of cancer cells with electrodes. The effect of Mebendazole(MBZ) drug, as a recently introduced anti tubulin agent induce mitotic arrest in cancer cells (Mukhopadhyay et al., 2002a), on the CV and DPV responses of the cells were investigated. The anodic/cathodic responses of SiNW biosensor to drug incubated MCF-7 cells with various doses and in various times were plotted by cyclic voltammetry (CV) and differential pulse voltammograms. Also, Confocal and flowcytometry assays were experimented as reference biological data for drug effects.

2. Materials and methods

2.1. Biosensor fabrication process

Silicon wafer substrates were cleaned through standard RCA #1 method (NH_4OH:H_2O_2:H_2O solution and volume ratio of 1:1:5 respectively). The surface of the wafer was then passivated using a thin layer (~ 300 nm) of SiO_2 grown by wet oxidation furnace. Gold catalyst layer with the thickness of 9 nm was coated on SiO_2 by sputtering system (Veeco Co.). The gold has been patterned by the architecture of integrate work, counter and reference electrodes. The radius of WE is about 35 μm. Then the sample was placed in LPCVD chamber and SiNW was grown as discussed in next sub section Finally, the sensors have been placed in a chamber made of plexi-glass and connected to potentiostat by conductive wires bonded to the its pads.

2.2. SiNW growth process

Details of the growth mechanism using the VLS technique are depicted in ref (Taghinejad et al., 2013). In summary, after cleaning n-type ⟨100⟩ silicon wafers using standard RCA#1 solution, a thin layer of gold (Au) catalyst with an approximately 5 nm thickness was deposited using sputtering (Veeco Co.) at a pressure of 20 mTorr.

Au-covered samples were located in a low pressure chemical vapor deposition (LPCVD) system with a quartz tube chamber. The growth is a two-step process named as graining and growth. During the graining, a thermal annealing at 450–550 °C for 30 min at the presence of argon (Ar) is carried out which results in the catalyst graining and formation of gold nano-sized islands. During the growth step, a mixture of high purity silane (SiH_4) as Si source and Ar as carrier and dilution gases were introduced to the chamber. Silicon crystalline nanostructures were formed on top of the catalyst islands in patterned region followed by breaking of the silane to Si and Si–H free radicals. In addition, a CM30 Phillips transmission electron microscope operated at 250 kV has been used to investigate the size and crystalline quality of the wires depend on growth parameters.

2.3. Cell culture and drug incubation

MCF-7 cell lines, obtained from the National Cell Bank of Iran (Pasteur Institute) had been isolated from grade I human breast tumors. Cells were maintained at CO_2 incubator (37 °C, 5% CO_2) in RPMI-1640 medium (Sigma) supplemented with 5% fetal bovine serum (Sigma), and 1% penicillin/ streptomycin (Gibco). The fresh medium was replaced every other day. Prior to each experiment, cells were trypsinized to be detached from the substrate and resuspended on the SiNW electrodes. To minimize the effect of trypsinization, the procedure was taken less than 4 min at room temperature around 20–22 °C. We held the samples in incubator for 4 h to achieve cells attachment on the SiNWs. Then the MBZ drug with lower (2.1 nM) and higher (10.5 nM) concentrations were added to individual samples. The signal recording and biological assays were investigated 2, 6 h and 10 h after the drug addition.

2.4. Electrochemical measurement procedure

For CV characterization, three-electrode electrochemical cyclic voltammetry was performed using the electrochemical workstation, RNFPG Stat (Roshd Nanofannavaran Co. Iran). Instead of the system electrodes, we used from our integrated electrodes fabricated as mentioned above. CV was performed between the integrated SiNW covered working and counter electrodes, with an on chip reference electrode. The reference electrode was calibrated before by Ag/AgCl reference electrode in 1 mM ferrocene carboxylic acid with 1 mM potassium chloride solution. CV studies were performed using DC voltage and no AC frequency was applied. For CV data recording, measurements were carried out at −0.8 to 0.8 V at a scan rate of 100 mV/s.

2.5. Confocal imaging

MCF-7 cells were grown on individual glass slides and treated with 2.1 and 10.5 nM MBZ for 2 h. In addition, CTRL sample was prepared as reference for comparison. Samples were then washed with PBS and permeabilized with microtubule stabilizing buffer [80 mM PIPES-KOH (pH 6.8), 5 mM EGTA, and 1 mM $MgCl_2$ containing 0.5% Triton X-100] for 5 min at room temperature before being fixed with chilled absolute methanol for 10 min at −20 °C. Fixed cells were washed and incubated with monoclonal mouse anti-α-tubulin antibody (Sigma) for 1 h at room temperature followed by incubation with FITC-conjugated antimouse IgG antibody (Santa Cruz Biotechnology). The stained cells were mounted with Vectashield (Vector Laboratories, Burlingame, CA) and observed by confocal microscopy.

2.6. Apoptosis and flowcytometric analysis of cell cycle

Apoptotic cells with characteristic nucleosomal DNA degradation were examined in none and MBZ treated cells. Drug treatment was carried for 2 h. Both floating and attached cells were harvested, and cell pellets were lysed in 100 μl of lysis buffer [10 mM Tris (pH 7.4), 10 mM EDTA (pH 8.0), and 0.5% Triton X-100]. The lysed pellets were then incubated for 10 min at 4 °C. DNA released in the supernatants was incubated with 200 μg/ml RNase A for 1 h at 37 °C and 200 μg/ml proteinase K for 30 min at 50 °C respectively. DNA was extracted and precipitated with 0.5 M NaCl and

50% isopropanol. The samples were loaded onto 2% agarose gels and stained with ethidium bromide. For cell cycle investigation by flowcytometry, cells were harvested, washed in PBS, and fixed in 70% methanol. The fixed cells were then incubated with 0.65 μg/ml mouse monoclonal anti-MPM-2 antibody. Cells were then incubated with 2 μg/ml FITC-conjugated goat antimouse IgG secondary antibody (Santa Cruz Biotechnology, Santa Cruz, CA), 20 μg/ml PI (Roche Diagnostics), and 10 μg/ml RNase A (Sigma-Aldrich) at 37 °C for 30 min and cell cycle analysis was performed using an EPICS Profile II flow cytometer (Coulter Corp., Miami, FL) with the Multicycle Phoenix Flow Systems program (San Diego, California).

3. Results and discussion

3.1. Characterization of SiNW structure

Fig. 1-A,B presents SEM images of the SiNW architecture in the shape of biosensors SiNWs grown at the presence of 20 Sccm of SiH_4 and a total pressure of 0.5 Torr have uniform distribution. The width of NWs is as narrow as 80 nm as measured by TEM imaging (Fig. S1-B). Ar has been used as a diluting gas with a flow rate of 1.2 l/min (SLM).

Bright field TEM image of the SiNWs is also shown in Fig. S1-B. The dark spots on the SiNW may be formed due to the catalyst migration during or after the growth period (Taghinejad et al., 2013). To investigate the crystallinity of the NWs, the obtained diffraction pattern of selected area (Fig. S1-C) reveals well defined diffraction spots, indexed as Si along the ⟨111⟩ zone axis. This result verifies the evolution of ⟨111⟩ directional growth. Based on this investigation, the nanowires have a well crystalline structure.

To corroborate the crystallinity of SiNW which directly affects its charge transfer properties, the Raman spectroscopy was experimented and presented in Fig. 1S-D. Observation of a peak at 528 cm^{-1} indicates the crystalline nature of the grown nanowires (Chen et al., 2007) which previously was studied by electron diffraction patterns (SAED).

Also it is important to note that the interactive surface of 1 μm^2 in bare Si electrode after covering by SiNW arrays would be increased to 1085 μm^2. Because more than 120 # wires with the length of 30 μm and radius of about 80 nm are existed on the 1 μm^2 surface of the electrode.

The morphology and configuration of the NWs formed a nest-like porous nanostructure with non-preferential orientations with respect to surface of the substrate (Fig. 1-B). Such morphology would provide unique electrochemical characteristics due to their high surface area and excellent ability of their boundaries in sensing any electrochemically produced charges through the crystally connected net of wires.

3.2. Characterization of SiNWEs by ferricyanide as reference ionic solutions

SiNWEs were analyzed by cyclic voltammetry at scan rate of 100 mV/s using 0.01 M of Ferricyanide ($[Fe(CN)_6]^{3-/4-}$) as reference and standard redox probe. The obtained result was shown in Fig. 2-A. The presence of both anodic and cathodic current peaks of SiNWEs located at 450 and 75 mV demonstrated the well electrochemical behavior of SiNWs with the great charge transfer mobility of nanowires. Also DPV response of $[Fe(CN)_6]^{3-/4-}$ covered on SiNW electrode exhibits a peak current of −58 nA.

3.3. Response of the sensors to the presence of cancer cells

To evaluate our integrated sensor in cell sensing approach, firstly the CV and DPV responses of the device were experimented in the presence of cells media solution as the crucial ionic environment existed in all of the measurements. Cells must be maintained and incubated in such media to being alive. RPMI1640 ionic solution (contained 10% FBS) is the cell culture media used in our investigation. So the electrochemical response of the media must be considered in all of experiments. The anodic response of RPMI detected by SiNWEs was located at 200 mV as shown in Fig. 2-C (curve (a)). The intensity of electrochemical DPV peak of RPMI sensed by SiNWs was −70 nA. High porosity/surface area of SiNWEs can help to increasing the detection resolution of any ionic transfer happened in the sensing media. After attachment of MCF-7 cells on the surface of SiNWE, both anodic and cathodic peaks of the CV response were decreased (Fig. 2-C curve (b)). It would strongly correlated with passivation of the electrodes by attached cells as dielectric layers.

Fig. 2-D (curve (b)) shows DPV profiles of the SiNWEs after attachment of the MCF-7 cells covered all of the effective surface of the electrode. By comparing this voltammogram with DPV spectra of RPMI solution (Fig. 2-D curve (a)), it is observable that the absolute DPV peak current in SiNWEs has reduced 14 times after attachment of the cells (from −70 to −5 nA). This would be a well indication on the high interactive surface of SiNWEs. Presence of the cells on the surface of SiNW electrodes suppressed the

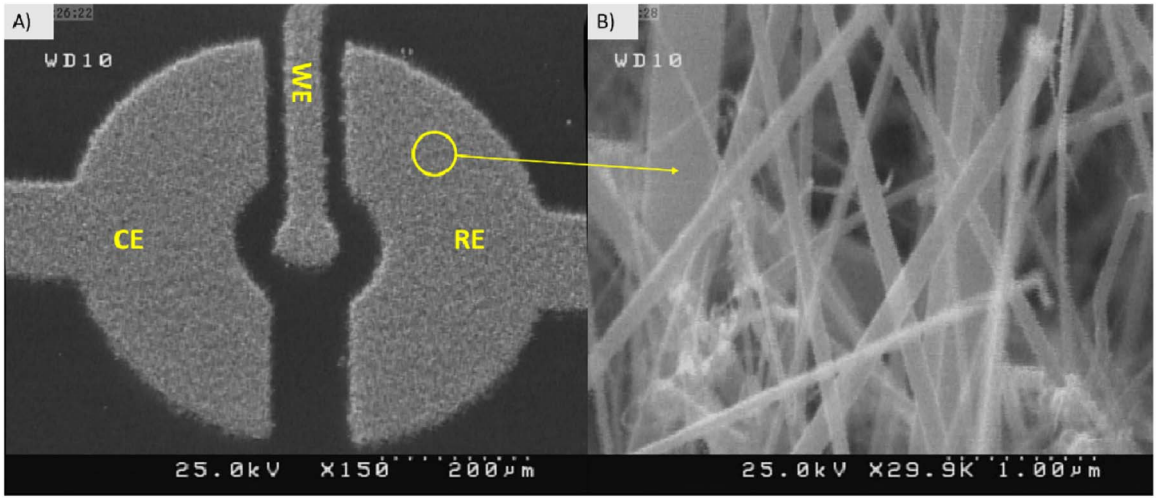

Fig. 1. A,B) FESEM image of SiNW biosensor. The NWs just existed in the patterned region.

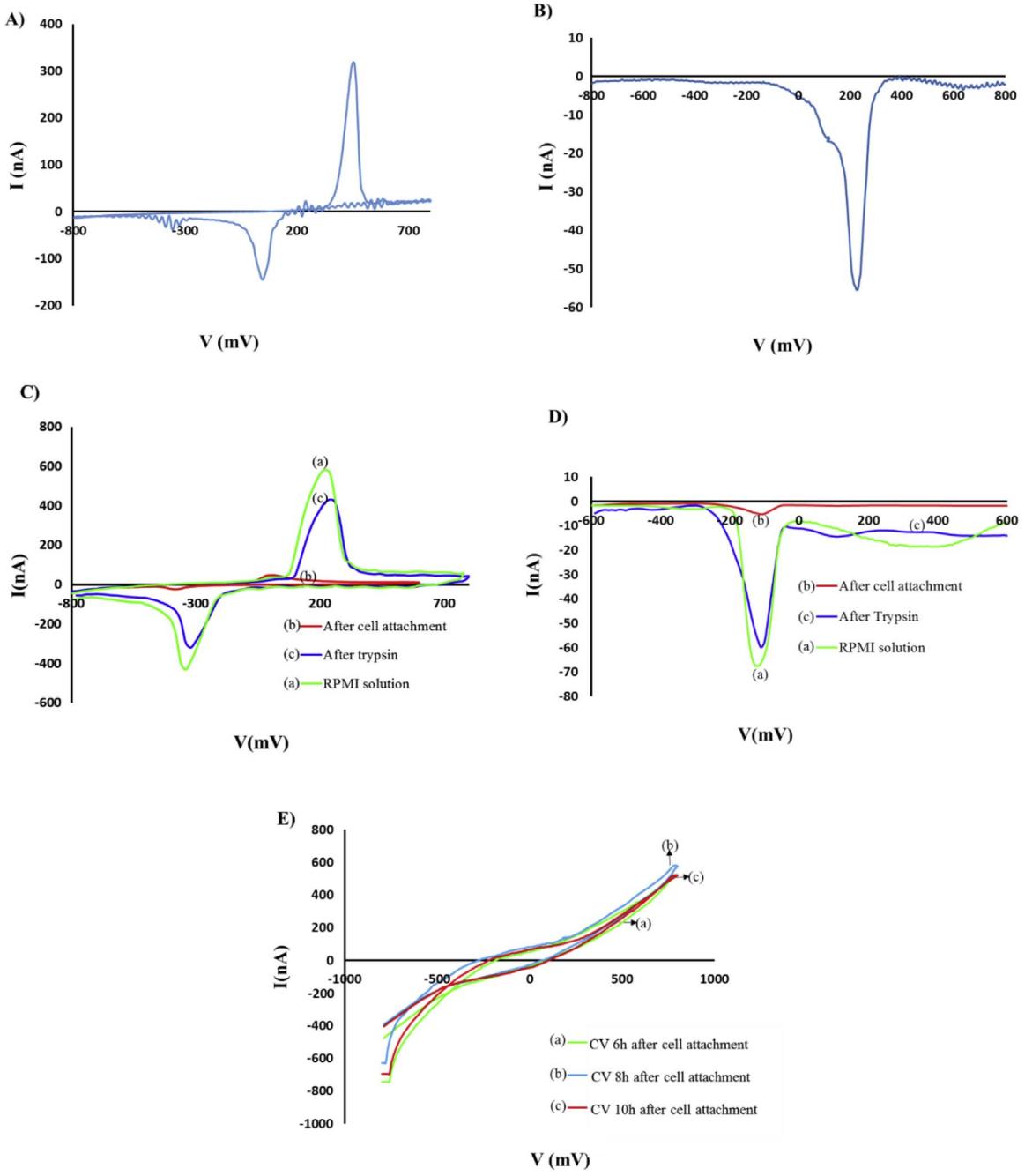

Fig. 2. A) CV and B) DPV of ferricyanide (K3Fe(CN)6) as standard ionic solution measured by SiNW electrochemical biosensor. C) CV and D) DPV of SiNW biosensor before and after attachment of MCF-7 cells as well as after their detachment from the surface by trypsin. E) CV response of cells attached on SiNWEs in various time laps. It presented the stable electrochemical state for the cells after attachment on the sensor.

current flow from WE to CE and degraded the DPV spikes. When detection is not mass transport constrained, only modest enhancement is expected at the lowest concentrations.

The measurements were repeated after detachment of the cells from the surface of SiNWE by trypsinization (as mentioned in Experimental Section). Fig. 2-C (curve (c)) presented that the anodic and cathodic spikes were again observed in the CV response of cells detached electrode. Also absolute DPV peak current increased (in negative regime) after detachment of the cells from 5 to 60 nA. Such increment would be certainly the result of removing the cells as the main agent of suppression in ionic transport between WEs and CEs. We can reveal that the remained adhesive proteins and some residues of the cells after trypsinization from the nanowires might inhibit from the precise adjustment of the peak current in its previous location (Fig. 2-D curve (c)) after detachment of the cells.

Monitoring the cells attached on SiNWEs in various time laps, indicated the stable ionic equilibrium induced by cells as no noticeable change was observed in the electrochemical behavior of the cells from 2hr to 6hr after their attachment on the surface (Fig. 2-E) As we know, the first 4hr is sufficient for the adhesion of cancer cells on NWs and after that the cells enter to spreading stage (Abdolahad et al., 2014b).

3.4. Shape and geometry of cancer cells attached on SiNWEs

Presence of cancer cells attached on the SiNWEs is observable in Fig. 3-B. The width distribution of skein structure of NWs

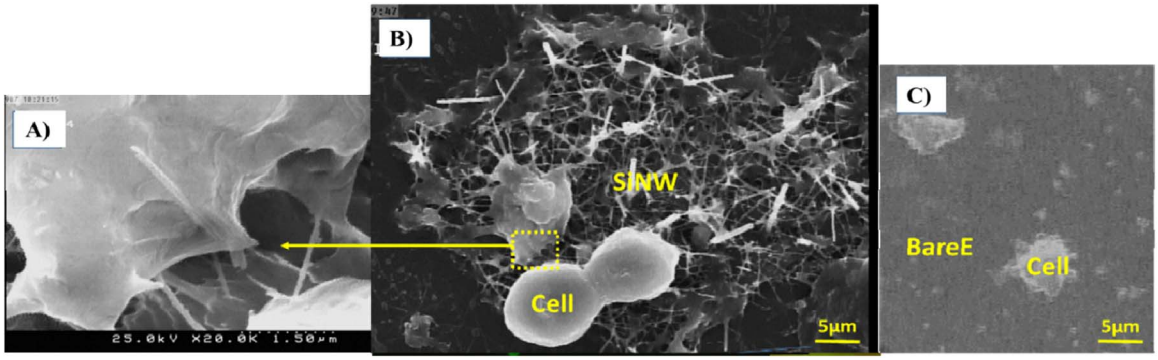

Fig. 3. A) FESEM image from MCF-7 cells attached on the surface of SiNWEs. The interactive interface between cancer cells and NWs is observable in panel A which is much higher than that of bare SiE (C).

ranged from 45 to 110 nm induced large efficient interactive surface between a cell and nanowires (Fig. 3-A) The efficient interactive surface of SiNWE in the region of a cell is about 22,700 μm^2 as can be measured from SEM images of Fig. 3-A, meanwhile such surface in bare Si electrode is about 127 µm2 (Fig. 3-C). The wires applied direct interaction with cells because of their attachment into outer membrane all of which considerably enhance the quality of the responses. Florescent microscopy images from green florescent protein (GFP) tagged cancer cells attached on NW arrays, shown in Fig. S2 indicated the vital state of the cells after interaction by the nanostructures. Expression of green color of proteins just would be related to live cells (Elliott and O'Hare, 1999). Also the trace of nanowires around a captured cell is observable in Fig. S2 (in situ).

3.5. Anticancer drug resistance assay of MCF-7 cells by SiNWEs

SiNWEs can also be used to electrochemically monitor the effect of any external biochemical stimulation on the vitality and function of the cells by tracking any ionic non-equilibrium induced in the sensors. Anticancer drugs are one of the clinically applicable biochemical stimulators of the cells. MBZ is an antitubulin drug induces tubulin depolymerization in cancer cells as mentioned above. We treated the MCF-7 cells attached on SiNWEs with different doses of MBZ and monitored the electrochemical response of individual CTRL and treated cells.

Fig. 4-A and B. presented the CV and DPV diagrams of CTRL and MBZ treated samples with individual concentrations of 2 and 10.5 nM respectively. Both anodic and cathodic spikes were observed in CV diagrams just 2hr after drug incubation with the cells.

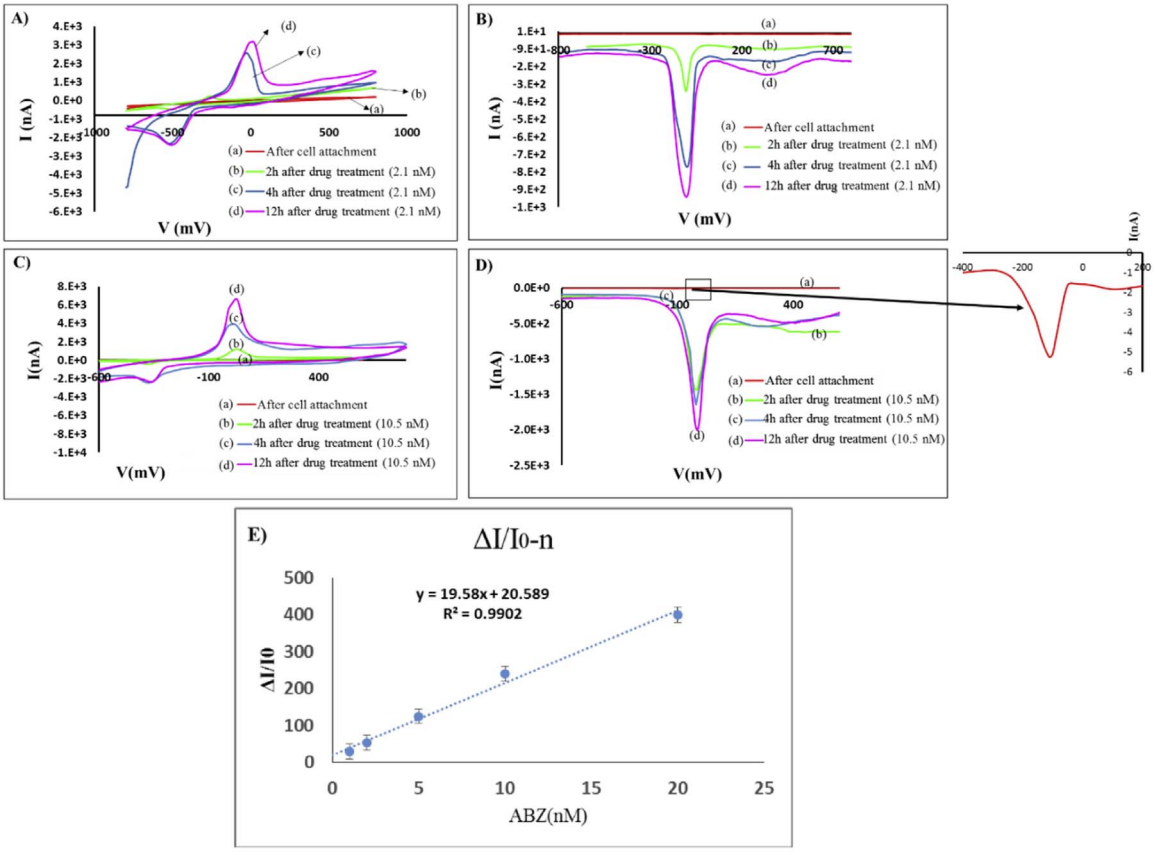

Fig. 4. A) CV and B) DPV spectra of MCF-7 cells attached on SiNW biosensor in various time lapses after interaction with 2.1 nM of MBZ. Similar experiment were done for individual sample treated with 10.5 nM of MBZ and results were obtained in panels (C) and (D) respectively. E) Detection limit profiles of the sensor for sensing the effect of MBZ on MCF-7 cells.

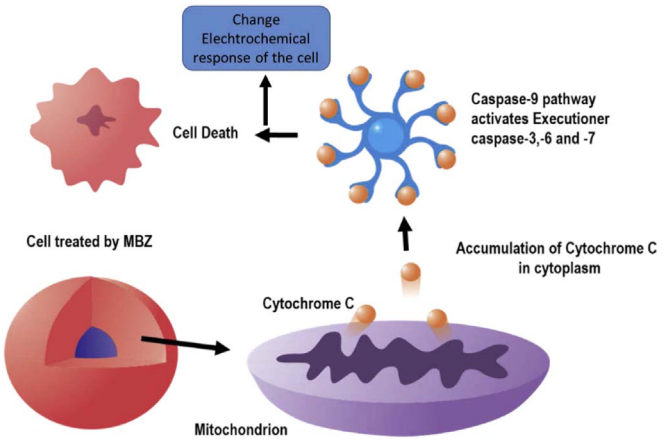

Fig. 5. Schematics from the electrochemical effect of MBZ on MCF-7 cells. Accumulation of cytochrome C from the mitochondria to the cytoplasm resulted in perturbation of the cell's ionic or electrochemical state.

Fig. 4-B indicated that just 2 nM of MBZ seriously affect the electrochemical response of cancer cells in 2 h. Absolute DPV current peaks of the sensor just 2 h after cells treatment by 2 nM of MBZ increased from 5 nA to 300 nA. 12 h after the treatment, the intensities of the absolute DPV peaks reached to 900 nA. By increasing the dose of MBZ to 10 nM, the height of the CV spikes increased by nearly three orders (Fig. 4-C). Absolute DPV of higher dose MBZ (10 nM) treated cells increased to 1400 and 2000 nA after 2 and 12 h respectively. Sharp electrochemical response of MBZ treated MCF-7 cells might be assigned to cells functional perturbations caused by drug induced Microtubule depolymerization. The great charge mobility among the net of nanowires, the excellent capability for exchange of electrons at the nanowalls, the ballistic mobility of electrons in silicon nanocrystalline structure and/or direct attachment of thin rounded nanowalls into the cells might all be effective in the well response of SiNWEs to electrochemical variations in drug treated cancer cells.

3.6. Detection limit

To check the reliability of the lower limit of detection in practice, we studied detection limit profiles of the sensor by various doses of MBZ (Fig. 4-E). By plotting the $\Delta I/I_0$ vs concentration of MBZ. Shows current response ($\Delta I/I_0$) defined as ratio of the current peak (obtained after subtraction of the background current in DPV) to the typical current resolution (here, 1 nA)) of the SiNWEs to the cancerous cells treated by MBZ at the various concentrations. It indicates that the SiNWEs can efficiently detect the dose dependent effect of drug on cancer cells with a linear behavior in the concentration range of 1–20 nM. By linear fitting the experimental data, the following equation (in situ of Fig. 4-E) was obtained for average of the current response as a function of drug concentration. Detection limit would be the drug doses less than 0.01 nM induce about 70 nA changes in the response of the sensor which completely overlapped by the response of the solution media. Also we defined a figure of merit for sensitivity per concentration of the MBZ discussed in SI.

3.7. Electrochemical Mechanism of drug effect

Many hypotheses were reported about the action mechanism of anti-tubulin drugs on cancer cells, all of which indicated on activation of one or more cellular signaling pathways such as Bcl phosphorylation, caspase3, 8 and 9 (Ona and Shibata, 2010), p53 (Wang and Sun, 2010) and release of cytochrome C from mitochondrial membrane to cytoplasm (Pantziarka et al., 2014). By investigating all of the mentioned pathways, we understood that the joint parameter in all of the pathways is alteration of cell's ionic state. As the result, we concluded that MBZ treatment would change the anodic/cathodic response peaks of the biosensor covered by cancer cells. Moreover, caspase inhibition was frequently found to prolong the duration of mitosis (Gascoigne and Taylor, 2009). Some investigations reported consecutive activation of more than one pathway as exposure to MBZ caused cytochrome c accumulation, activation of caspase-9 and caspase-8, and cleavage of PARP and procaspase-3 (Pantziarka et al., 2014).

Some, reports revealed that the fastest MBZ signaling goes through the mitochondrial Pathway. Accumulated Cytochrome C in cytosolic region of MBZ treated cells, increased in a dose-dependent manner. After 12 h from this accumulation, activation of caspase-9 and caspase-8 and cleavage of the caspase substrate poly(ADP-ribose) polymerase and procaspase-3 were detectable (Mukhopadhyay et al., 2002b).

Based on above pathways, the changed electrochemical response of the SiNWEs after treating the cells by MBZ could be translated in a well demanded electrochemical approach. The result of released cytochrome C (as an active ionic agent (oxidative)) from mitochondrial membrane into cytoplasm would change the ionic state of cytoplasm and subsequently the ionic equilibrium between cell's inner and outer parts (Fig. 5). Also it has been reported that released cytochrome C would be chemically reduced so fast in cytoplasm of MBZ treated cells (Ripple et al., 2010). This result completely indicated our hypothesis on affected electrochemical and changed anodic/catholic responses of the cells covered SiNWEs after the drug treatment.

As seen in Fig. 4, the DPV peaks of cancer cells incubated with low and high doses of MBZ indicated that increasing the dose of MBZ resulted in further releasing of Cytochrome C and sharper changes in anodic response of the cancer cells.

Our suggested mechanism is in a well corroboration with the illustrious fact that, depolymerization of MTs by MBZ, alters membrane potential and disturbs the motional freedom of membrane proteins (Herold and Rasooly, 2012) resulted in perturbing the function of Na^+ ion channels.

3.8. Confocal and flowcytometry assays of drug treated cancer cells

Confocal imaging taken from MBZ treated cells (Fig. 6) corroborated the disorders in tubulin assemblies in comparison with non-treated cells which indicated the activation of tubulin depolymerizing pathways. Release and reduction of Cytochrome C in cytoplasm might affect the microtubule associated proteins (Such as LC3 (Tanida et al., 2008) and perturb the depolymerization rate of MTs. Images taken from untreated cells revealed that normal bipolar spindles were observed in cytoskeletal structure (Fig. 6-A). But in MBZ treated sample, cells had abnormally reduced numbers of spindles or monopolar (monoaster) spindles (Fig. 6-B).

In addition, Cell cycle progression in control and drug treated samples determined by flowcytometry analysis confirmed that various concentrations of MBZ induced non similar effects on the cycles and states of the cells. As presented in Fig. 6-C, the subG_1 fraction, represents apoptotic cells with hypodiploid DNA (Pan et al., 2014; Aszalos et al., 1986), increased a little in drug treated samples (Apoptotic part in Figs. 6-C-1 and 2). This reveal that MBZ (2.1 nM) didn't induce the apoptotic behavior of MCF-7 cells. But proportion of G_0/G_1 fraction changed in MBZ incubated samples. The peak of G_0/G_1 was 1300 in CTRL sample (Figs. 5-C-1) meanwhile it was reduced to 800 in MBZ (2.1 nM) treated cells (Figs. 5-C-2). The result was confirmed by side scatter versus forward scatter (SSC-FSC) diagram as a strong sign of cells granularity (Aszalos et al., 1986) (Right panels in Fig. 6 C-1-C-3). Also the G_2/M fraction in MBZ (2 nM) treated sample (Fig. 6-C-2) was less than

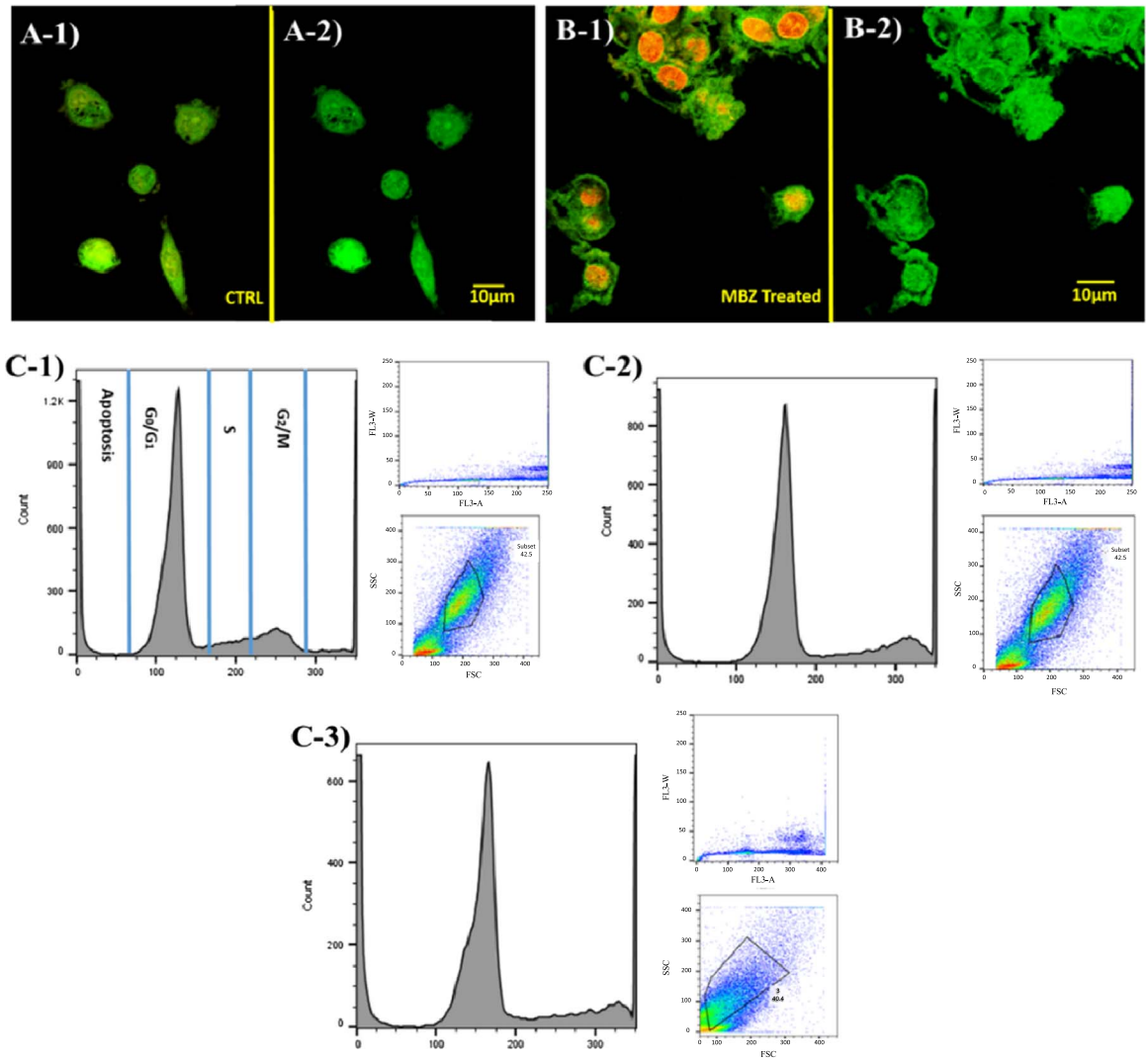

Fig. 6. Confocal microscopy images from the tubulin assemblies of MCF-7 cells in (A) CTRL state in comparison with (B) the cells treated by 2.1 nM of MBZ in same times. The duration of incubation with drugs was 2 h. Extensive depolymerization rate in MTs resulted in non-regular spindle formation in MBZ treated samples the trace of the PI tagged nucleus is observable in panels A-1 and B-1 in orange color. Also, flowcytometry analyses of MCF-7 cells in (C-1) No drug, (C-2) MBZ 2.1 nM and (C-3) MBZ 10,5 nM treated states were presented. The cell's fractions in apoptotic, G_0/G_1, S and G_2/M cycles are observable in all of panels. MBZ treatment reduced the vitality of the cells and perturb the cells cycle. R1 region (presented in the right of each panels) indicated the state of counted cells. (For interpretation of the references to color in this figure legend, the reader is referred to the web version of this article.).

half of measured for CTRL. By increasing the doses of MBZ to 10.5 nM, apoptotic behavior of the cells was affected. Also, sharper reduction in the amount of the cells in G_0/G_1 phase was observed in similar time (Figs. 6-C-3). Such disorders in the cycle of the cells after MBZ treatment would be well demanded by affected anodic/cathodic response of the cells measured by SiNWEs.

4. Conclusion

In summary, silicon nanowire biosensor (in an integrated architectures of work, counter and reference electrodes) was fabricated and applied to detect the electrochemical response of breast cancer cells to MBZ anti tubulin drugs. MBZ perturbs the anodic/cathodic response of cells covered biosensor by releasing Cytochrome C in cytoplasm. The changed redox/oxidative behavior of the cells, initiated from the reduction of cytochrome C, would be detected by monitoring the CV and DPV of SiNW biosensor. By applying well direct bioelectrical contacts with cancer cells, SiNWs can amplify signal transduction and detect the biological effect of low doses MBZ on MCF-7 cells. The device detected the trace of 2 nM MBZ by exhibiting 250 nA changes in DPV peak of the sample. As future application, this device could be applied as a new label-free instrument for extreme drug resistance assay.

Appendix A. Supporting information

Supplementary data associated with this article can be found in the online version at http://dx.doi.org/10.1016/j.bios.2016.04.081.

References

Abdolahad, M., Shashaani, H., Janmaleki, M., Mohajerzadeh, S., 2014a. Silicon nanograss based impedance biosensor for label free detection of rare metastatic cells among primary cancerous colon cells, suitable for more accurate cancer staging. Biosens. Bioelectron. 59, 151–159. http://dx.doi.org/10.1016/j.bios.2014.02.079.

Abdolahad, M., Janmaleki, M., Taghinejad, M., Taghnejad, H., Salehi, F., Mohajerzadeh, S., 2013. Single-cell resolution diagnosis of cancer cells by carbon nanotube electrical spectroscopy. Nanoscale 5, 3421–3427. http://dx.doi.org/10.1039/c3nr33430a.

Abdolahad, M., Taghinejad, H., Saeidi, A., Taghinejad, M., Janmaleki, M.,

Mohajerzadeh, Z., 2014. Cell membrane electrical charge investigations by Silicon nanowires incorporated Field Effect Transistor (SiNWFET) suitable in cancer research. RSC Adv. 4, 7425. http://dx.doi.org/10.1039/c3ra46272b.

Aszalos, A., Damjanovich, S., Gottesman, M.M., 1986. Depolymerization of microtubules alters membrane potential and affects the motional freedom of membrane proteins. Biochemistry 25, 5804–5809.

Bauer, J., Fleischer, F., Breitenstein, O., Schubert, L., Werner, P., Gösele, U., Zacharias, M., 2007. Electrical properties of nominally undoped silicon nanowires grown by molecular-beam epitaxy. Appl. Phys. Lett. 90, 012105. http://dx.doi.org/10.1063/1.2428402.

Chen, K.-I., Li, B.-R., Chen, Y.-T., 2011. Silicon nanowire field-effect transistor-based biosensors for biomedical diagnosis and cellular recording investigation. Nano Today 6, 131–154. http://dx.doi.org/10.1016/j.nantod.2011.02.001.

Chen, Y., Peng, B., Wang, B., 2007. Raman spectra and temperature-dependent raman scattering of silicon nanowires. J. Phys. Chem. C 111, 5855–5858. http://dx.doi.org/10.1021/jp0685028.

Elliott, G., O'Hare, P., 1999. Live-cell analysis of a green fluorescent protein-tagged Herpes simplex virus infection. J. Virol. 73, 4110–4119.

Gascoigne, K.E., Taylor, S.S., 2009. How do anti-mitotic drugs kill cancer cells? J. Cell Sci. 122, 2579–2585. http://dx.doi.org/10.1242/jcs.039719.

Guo, Y., Guo, Y., Dong, C., 2013. Ultrasensitive and label-free electrochemical DNA biosensor based on water-soluble electroactive dye azophloxine-functionalized graphene nanosheets. Electrochim. Acta 113, 69–76. http://dx.doi.org/10.1016/j.electacta.2013.09.039.

Gupta, R., Chaudhury, N.K., 2007. Entrapment of biomolecules in sol-gel matrix for applications in biosensors: problems and future prospects. Biosens. Bioelectron. 22, 2387–2399. http://dx.doi.org/10.1016/j.bios.2006.12.025.

Hepel, M., Zhong, C.-J. (Eds.), 2012. Functional nanoparticles for bioanalysis, nanomedicine, and bioelectronic devices vol. 1. In: Proceedings of the ACS Symposium Series, American Chemical Society, Washington, DC. ⟨http://dx.doi.org/10.1021/bk-2012-1112⟩.

Herold, Keith E., Rasooly, Avraham, 2012. Biosensors and Molecular Technologies for Cancer Diagnostics. CRC Press, FL.

Hosseini, S.A., Abdolahad, M., Zanganeh, S., et al., 2016. Nanoelectromechanical chip (NELMEC) combination of nanoelectronics and microfluidics to diagnose epithelial and mesenchymal circulating tumor cells from leukocytes. Small 12, 883–891. http://dx.doi.org/10.1002/smll.201502808.

Jacobs, C.B., Peairs, M.J., Venton, B.J., 2010. Review: carbon nanotube based electrochemical sensors for biomolecules. Anal. Chim. Acta 662, 105–127. http://dx.doi.org/10.1016/j.aca.2010.01.009.

Kimmel, D.W., LeBlanc, G., Meschievitz, M.E., Cliffel, D.E., 2012. Electrochemical sensors and biosensors. Anal. Chem. 84, 685–707. http://dx.doi.org/10.1021/ac202878q.

Kong, R.-M., Song, Z.-L., Meng, H.-M., Zhang, X.-B., Shen, G.-L., Yu, R.-Q., 2014. A label-free electrochemical biosensor for highly sensitive and selective detection of DNA via a dual-amplified strategy. Biosens. Bioelectron. 54, 442–447. http://dx.doi.org/10.1016/j.bios.2013.11.041.

Li, F., Peng, J., Wang, J., Tang, H., Tan, L., Xie, Q., Yao, S., 2014. Carbon nanotube-based label-free electrochemical biosensor for sensitive detection of miRNA-24. Biosens. Bioelectron. 54, 158–164. http://dx.doi.org/10.1016/j.bios.2013.10.061.

Mukhopadhyay, T., Sasaki, J., Ramesh, R., Roth, J.A., 2002a. Mebendazole elicits a potent antitumor effect on human cancer cell lines both in vitro and in vivo. Clin. Cancer Res. 8, 2963–2969.

Mukhopadhyay, T., Sasaki, J., Ramesh, R., Roth, J.A., 2002b. Mebendazole elicits a potent antitumor effect on human cancer cell lines both in vitro and in vivo. Clin. Cancer Res. 8, 2963–2969.

Ona, T., Shibata, J., 2010. Advanced dynamic monitoring of cellular status using label-free and non-invasive cell-based sensing technology for the prediction of anticancer drug efficacy. Anal. Bioanal. Chem. 398, 2505–2533. http://dx.doi.org/10.1007/s00216-010-4223-5.

Pan, Z., Avila, A., Gollahon, L., 2014. Paclitaxel induces apoptosis in breast cancer cells through different calcium–regulating mechanisms depending on external calcium conditions. Int. J. Mol. Sci. 15, 2672–2694. http://dx.doi.org/10.3390/ijms15022672.

Pantziarka, P., Bouche, G., Meheus, L., Sukhatme, V., Sukhatme, V.P., 2014. Repurposing drugs in oncology (ReDO)-Mebendazole as an anti-cancer agent. Ecancermedicalscience 8, 443. http://dx.doi.org/10.3332/ecancer.2014.443.

Prinz, C.N., 2015. Interactions between semiconductor nanowires and living cells. J. Phys. Condens. Matter 27, 233103. http://dx.doi.org/10.1088/0953-8984/27/23/233103.

Qi, S., Yi, C., Ji, S., Fong, C.-C., Yang, M., 2009. Cell adhesion and spreading behavior on vertically aligned silicon nanowire arrays. ACS Appl. Mater. Interfaces 1, 30–34. http://dx.doi.org/10.1021/am800027d.

Qing, Q., Jiang, Z., Xu, L., Gao, R., Mai, L., Lieber, C.M., 2014. Free-standing kinked nanowire transistor probes for targeted intracellular recording in three dimensions. Nat. Nanotechnol. 9, 142–147. http://dx.doi.org/10.1038/nnano.2013.273.

Qu, Y., Liao, L., Li, Y., Zhang, H., Huang, Y., Duan, X., 2009. Electrically conductive and optically active porous silicon nanowires. Nano Lett. 9, 4539–4543. http://dx.doi.org/10.1021/nl903030h.

Ripple, M.O., Abajian, M., Springett, R., 2010. Cytochrome c is rapidly reduced in the cytosol after mitochondrial outer membrane permeabilization. Apoptosis 15, 563–573. http://dx.doi.org/10.1007/s10495-010-0455-2.

Taghinejad, H., Taghinejad, M., Abdolahad, M., Saeidi, A., Mohajerzadeh, S., 2013. Fabrication and modeling of high sensitivity humidity sensors based on doped silicon nanowires. Sens. Actuators B Chem. 176, 413–419. http://dx.doi.org/10.1016/j.snb.2012.09.062.

Tanida, I., Ueno, T., Kominami, E., 2008. LC3 and Autophagy. Methods Mol. Biol. 445, 77–88. http://dx.doi.org/10.1007/978-1-59745-157-4_4.

Turner, M., Londei, M., Feldmann, M., 1987. Human T cells from autoimmune and normal individuals can produce tumor necrosis factor. Eur. J. Immunol. 17, 1807–1814. http://dx.doi.org/10.1002/eji.1830171220.

Wang, Z., Sun, Y., 2010. Targeting p53 for novel anticancer therapy. Transl. Oncol. 3, 1–12.